Catalysis Today 147S (2009) S324–S329

Contents lists available at ScienceDirect

Catalysis Today

journal homepage: www.elsevier.com/locate/cattod

An internally illuminated monolith reactor: Pros and cons relative to a slurry reactor

Joana T. Carneiro [a], Rob Berger [b], Jacob A. Moulijn [a], Guido Mul [a,*]

[a] Department of Catalysis Engineering, Delft University of Technology, Julianalaan 136, Delft, 2628 BL, The Netherlands
[b] Anaproc, Julianalaan 136, Delft, 2628 BL, The Netherlands

ARTICLE INFO

Article history:
Available online 8 August 2009

Keywords:
Modeling
Photoreactor
Optical fibers
Light profile

ABSTRACT

In the present study, kinetic models for the photo-oxidation of cyclohexane in two different photoreactor systems are discussed: a top illumination reactor (TIR) representative of a slurry reactor, and the so-called internally illuminated monolith reactor (IIMR) representing a reactor containing immobilized catalyst. Results show that the models considered for both reactors predict the experimental values well. The IIMR is shown to be a better design in terms of light delivery at the catalyst surface. For the same photon power (Einst s^{-1}) the IIMR will perform at lower photon irradiance (Einst m^{-2} s^{-1}) since the area exposed to the light is higher. It will be shown that the catalyst can thus be used more efficiently in the IIMR.

1. Introduction

One of the challenges in the research field of photocatalysis is developing reactors, allowing an optimized photonic efficiency [1]. Various designs have been evaluated to resolve the light distribution problem in photoreactors, including those containing immobilized photocatalysts [2,3]. One approach is to employ optical fibers as a light distributing guide and support for photocatalysts. A recent example of this concept is the optical fiber monolith reactor, as reported by Lin and Valsaraj [4]. They used a monolith for photocatalytic wastewater treatment with the channels of the monolith completely filled with flowing liquid. The monolith structure was used merely as the distributor of the optical fibers, while the benefits of monolith, such as low pressure drop and excellent mass transfer characteristics for gas/liquid systems in certain hydrodynamic regimes, were not fully exploited to optimize the photocatalytic oxidation reaction [5]. In our laboratory, the so-called internally illuminated monolith reactor (IIMR) was developed [6]. In this reactor system, the optical fibers are tip-coated with a reflective material and the catalyst is coated on the walls of the monolith, which decouples the light propagation process in the fiber from the physical properties of the catalytic layer. With the side-light fibers illuminating the coated walls of the monolith channels from the front, reactant concentration and light intensity decay from the external surface towards the ceramic wall of the monolith, with their maximum value at the photocatalyst surface. This affects the photonic efficiency, for a batch system, of the reactor positively, Eq. (1):

$$\xi = \frac{\text{reaction rate}\,(\text{mol}\,s^{-1})}{\text{photon flow}\,(\text{Einst}\,s^{-1})} = \frac{dn/dt}{AI''} \quad (1)$$

In this equation, for a batch reactor, n is the number of moles converted (mol), t is the time (s), A is the area through which light propagates into the reactor (m^2), and I'' is the photon flux (Einst m^{-2} s^{-1}). Note that we use here for convenience a definition of the rate that is not normalized to the amount of catalyst.

In the present paper we propose a kinetic model for cyclohexane oxidation in the reactor system based on side light emitting fibers. The tip-coated 'side-light fibers' are evenly distributed inside the ceramic (i.e. cordierite) monolith structure, on the inner walls of which titania photocatalyst has been coated [6]. The top illumination reactor (TIR), representative for a reactor containing a slurried catalyst, is modelled for comparison.

Experimental results obtained for the selective photo-oxidation of cyclohexane in both reactors are used to evaluate the models. The selective photocatalytic oxidation of cyclohexane in liquid phase to cyclohexanone is of particular interest for industry. Cyclohexanone is the precursor of caprolactam, a monomer for the nylon-6 production. High ketone selectivities were reported by several authors [7–12] in the photo-oxidation of cyclohexane, if highly energetic UV light of low wavelengths is prevented to enter the reactor [13]. In the present study a wavelength of 367 nm was therefore used in the model evaluation.

* Corresponding author.
E-mail address: G.Mul@tudelft.nl (G. Mul).

0920-5861/$ – see front matter © 2009 Elsevier B.V. All rights reserved.
doi:10.1016/j.cattod.2009.07.041

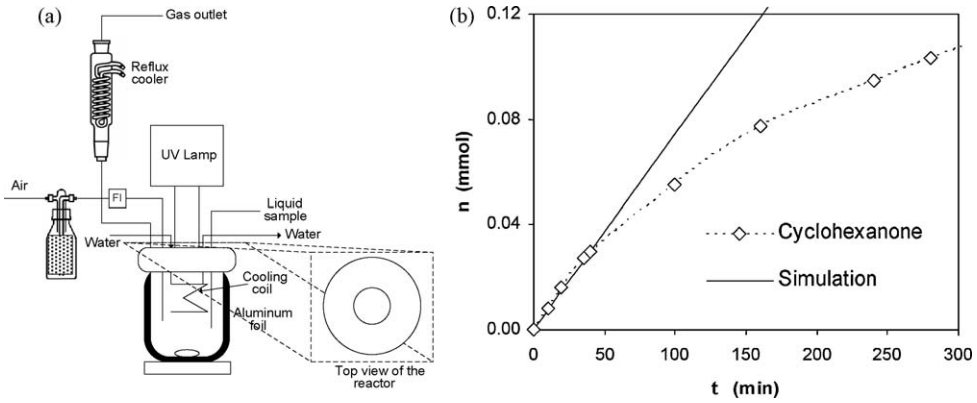

Fig. 1. (a) Schematic representation of the top illumination reactor (TIR). (b) Product (cyclohexanone and cyclohexanol) evolution with time in the TIR and simulation results.

2. Experimental

2.1. Photocatalyst

The TiO_2 used in the photocatalytic tests in the IIMR and TIR was Hombikat UV100 (100% anatase as determined by XRD) with a 337 $m^2\ g^{-1}$ surface area and a mean agglomerate size in cyclohexane of $\pm 3\ \mu m$ [13]. For immobilizing TiO_2 on the monolith walls, the washcoat procedure reported previously [14] was used. The final amount of TiO_2 present in the monolith was ~17 g, yielding an estimated layer thickness of ~80 μm. Detailed information concerning characterization of this coating is provided elsewhere [6].

2.2. Top illumination reactor: slurry system

Reactions were carried out in a top illumination reactor (Fig. 1a) as described previously [15]. In a typical experiment 100 mL of cyclohexane containing 1 g L^{-1} of finely dispersed TiO_2 (anatase) catalyst (average agglomerate size = 3.0 μm, particle porosity = 0.5, solid material density = 3840 kg m^{-3}) was used. The catalysts were dried for 1 h at 120 °C to remove adsorbed water and impurities. The solution was illuminated from the top of the reactor through a Pyrex window, having a diameter of 2.6 cm, that cuts off the highly energetic UV radiation [13]. A high pressure mercury lamp of 50 W was used (HBO50W from ZEISS). The light intensity of the lamp in the wavelength absorption range of TiO_2 (275–388 nm) is 55 mW cm^{-2} at the lamp surface, which corresponds to a light flux of 1.8×10^{-3} Einst $m^{-2}\ s^{-1}$ entering the reactor. Air presaturated with cyclohexane, dried over Molsieve 3 Å (Acros Organics), was bubbled through the TiO_2 suspension at a rate of 30 mL min^{-1}. During the reaction 0.2 mL liquid samples were withdrawn for GC analysis. Organic compounds were quantatively analyzed twice using a gas chromatograph with a flame ionization detector (Chrompack, CPwax52CB). Hexadecane was used as an internal standard. Since cyclohexanone is formed with a high selectivity of >98%, only cyclohexanone production obtained in this reactor is presented in Fig. 1b. After about 60 min the catalyst starts to deactivate, which will not be further discussed here [13].

2.3. Internally illuminated monolith reactor: immobilized system

The IIMR consists of side light optical fibers, diameter 0.45 mm, located inside the 44 channels of a 25 cm long monolith. Before entering the quartz fiber guides, the light passes through a Pyrex window to cut off the highly energetic UV radiation. The square monolith channels have an internal size of 4.3 mm. A 55 mm long diffuser causes an equal distribution of the light over all the fibers. A mirror coating at the end of the side-light optical fibers causes the light to be reflected, resulting in an almost constant side-light intensity all over the length. The radiant flux at the fiber surface amounts to 13.8 mW cm^{-2}, independent of the axial distance from the light source. This irradiance (i.e. light flux) corresponds to 4.7×10^{-5} Einst $m^{-2}\ s^{-1}$. Without application of the mirror coating at the end of the fibers the side-light intensity dropped dramatically. The reactor is operated in semibatch mode; the liquid volume amounts to 800 mL of pure cyclohexane which is continuously recirculated through the monolith with a total flow rate of 0.5 L min^{-1}. The cocurrent downward flow rate of air, presaturated with cyclohexane in the liquid recirculation vessel, was 15 L min^{-1}. The liquid enters the monolith channels through a spray nozzle in order to achieve a good distribution in all the monolith channels. Fig. 2a shows a scheme of this reactor with enlarged schematic drawings of the fiber optic bundle and the monolith channels. The data on product formation previously obtained by Du et al. [6] are presented in Fig. 2b.

3. Modeling

3.1. Catalyst effectiveness

Due to the absorption of the UV light by the TiO_2 catalyst material, the light flux decreases inside the catalyst, following the Lambert–Beer law. Since the catalyst particles and the catalytic coating contain pores, which do not contribute to the light absorption, the light intensity profile inside the catalyst particles or coating follows from Eq. (2):

$$I''_x = I''_s \exp(-(1-\varepsilon_p)bx) \text{ with } b = 4\pi\frac{kn}{\lambda} \quad (2)$$

where I''_x is the irradiance (i.e. photon flux) at a depth x inside the TiO_2 layer or particle (Einst $m^{-2}\ s^{-1}$), I''_s is the photon flux at the surface of the TiO_2 (Einst $m^{-2}\ s^{-1}$), ε_p is the catalyst porosity, b is the overall extinction coefficient of non-porous TiO_2 (m^{-1}), x is the distance from the surface of the particle or coating (m), k is the index of absorption of non-porous TiO_2, n is the index of refraction and λ is the wavelength of the radiation (m).

The index of absorption, k, of the UV light in TiO_2 depends on the wavelength λ; for λ = 300 nm it amounts to 1.0 and for λ = 367 nm it amounts to 0.05 [16]. The index of refraction, n, is not as wavelength dependent as k and has the value of ~2.4. This corresponds to b values of 1.01×10^8 and $4.11 \times 10^6\ m^{-1}$, respectively. For the penetration depth (d_{pen}), defined as the depth where 99% of the light intensity is absorbed, applies:

$$d_{pen} = \frac{\ln(100)}{(1-\varepsilon_p)b} \quad (3)$$

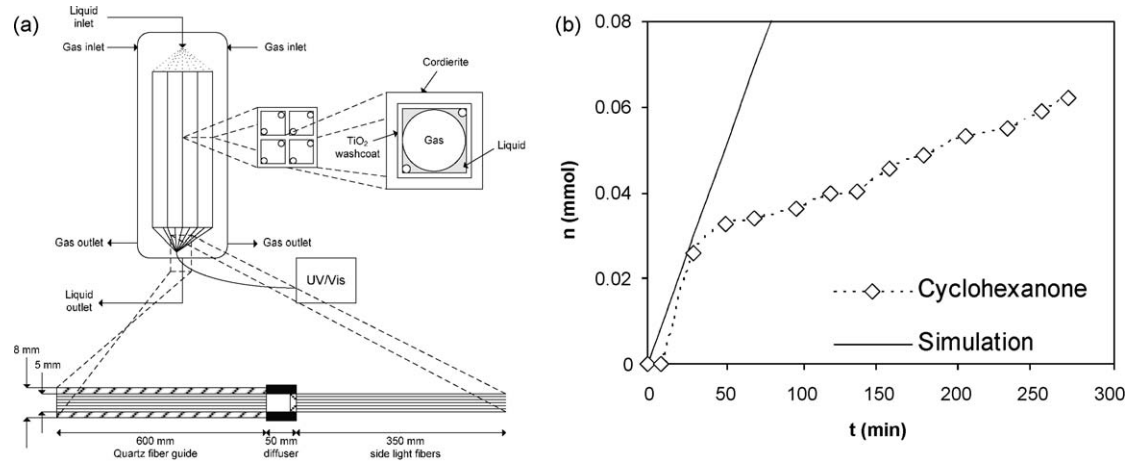

Fig. 2. (a) IIMR scheme with a detail of the cross-section of the monolith channels and the fiber optic bundle. (b) Product evolution with time in the IIMR.

Using a typical catalyst porosity of 0.5, d_{pen} is 0.031 μm at λ = 300 nm, and d_{pen} is 2.20 μm at λ = 367 nm. For the reactor modeling it is assumed for simplicity that the radiation is monochromatic with a wavelength of 367 nm, according to the lamp emission spectrum shown in Fig. 3. Although the lamp spectrum shows a wider emission range, the TiO_2 absorption range is limited to 275–388 nm which corresponds to the emission peak of the lamp at 367 nm.

It has been reported that the dependency of the chemical reaction rate on the light intensity is linearly proportional with the energy light flux up to a power flux of 25 mW cm^{-2} [17]; above this value the reaction rate becomes proportional to the square root of the irradiance. This means that recombination of charge carriers in the photocatalyst occurs to a significant extent at higher light intensity and not all the photo-generated electron–hole pairs are being used for the reaction. This has also been observed in conductance measurements using the time resolve microwave conductivity technique [18,19]. Using the wavelength of 367 nm and Eq. (4), this threshold value corresponds to an irradiance of 8.0×10^{-4} Einst m^{-2} s^{-1}:

$$I'' = \frac{E\lambda}{chN_A} \tag{4}$$

where I'' is the photon flux (Einst m^{-2} s^{-1}), E is the power flux (W m^{-2}), λ is the wavelength (m), c is the speed of light (3.0×10^8 m s^{-1}), h is the Planck's constant (6.63×10^{-34} J s) and N_A is the Avogadro's number (6.02×10^{23} mol^{-1}).

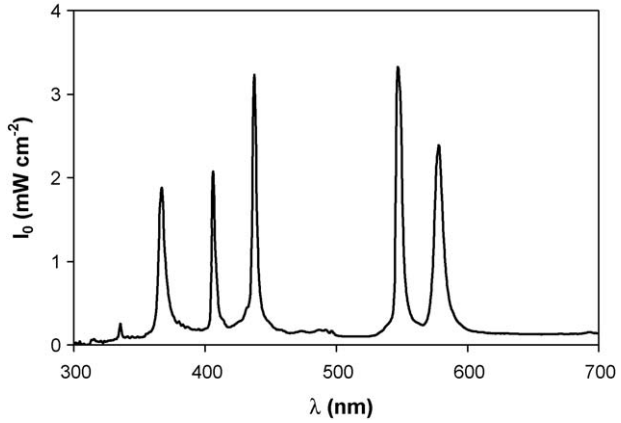

Fig. 3. Light intensity emission spectra of the lamp used in the TIR.

In the model the dependency of the chemical reaction rate with the radiance flux is set to a power m, which can be fitted from experimental data obtained in the TIR. The light intensity entering this reactor was varied between 5.11×10^{-4} and 5.11×10^{-3} Einst m^{-2} s^{-1} (determined using a spectrophotometer, Avantes). In Fig. 4 the variation of the reaction rate with light intensity, at the liquid surface, in the TIR is shown. In this case the light intensity is linearly proportional to the power flux until ~20 mW cm^{-2}. Above this value the reaction rate becomes proportional to the square root of the power flux. According to what is indicated in Fig. 4, the value of m for both reactors is considered to be 1 meaning that the light flux is limiting the reaction.

The local reaction rate r_j is expressed using a simple power-law expression:

$$r_j = (I_x'')^m k_j C_{sites} C_A^n \tag{5}$$

where r_j is the rate of reaction j ($mol_A\ m_{cat}^{-3}\ s^{-1}$), m is the power of the light intensity in the reaction rate, k_j is the rate constant of reaction j ($((\text{Einst}\ m^{-2}\ s^{-1})^{-m}\ m^{3n}\ mol_A^{1-n}\ mol_{sites}^{-1}\ s^{-1}$), C_{sites} is the concentration of active sites in the catalyst layer ($mol_{sites}\ m_{cat}^{-3}$), C_A is the concentration of reactant A ($mol_A\ m^{-3}$), and n is the reaction

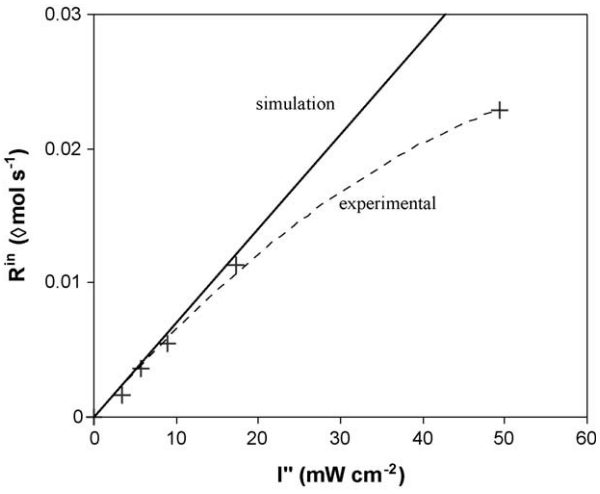

Fig. 4. Experimental and simulation (model) data of the initial reaction rate dependency with light flux in the TIR. The light intensity measured at the reactor entrance was multiplied by the factor $(d_{lamp}/d_{reactor})^2$ to have the light intensity at the liquid surface.

order with respect to the reactant. The value of C_{sites} was estimated from ammonia TPD and amounts to 0.5 mol kg^{-1} [15].

It is known that the reaction used in this work, cyclohexane selective photocatalytic oxidation, gives as main product cyclohexanone (high selectivity compared to cyclohexanol) and that deactivation occurs in early stages of the reaction due to carboxylate formation [6,13,20]. To simplify the modeling, the deactivation was not taken into account but only the initial rate of cyclohexanone formation. Since catalyst deactivation in the studied reaction causes the rate to decrease rather quickly, the fitting for determining k_j from the experimental data (obtained in the TIR) has an error associated and will not be ideal. Furthermore, this reaction is very slow with low TOF (min^{-1}) values, thus not diffusion limited. When the amount of photons is limiting the reaction rate, C_{sites} should have an exponent equal to zero. The amount of sites is often higher than the photons reaching the catalyst surface, corresponding with this zero-order behavior. Similarly, the reactant concentration C_A can be assumed to be constant, when (i) the conversion is as low as reported in this study and (ii) the reactant is the liquid reaction medium. Under these circumstances, the kinetic equation can be simplified to $r_j = k_{app}(I''_x)^m$.

3.2. TIR

The top-illuminated batch reactor consists of a well-stirred tank with finely dispersed catalyst particles. If, for simplicity, it is assumed that the particles have a cubic shape and that they are always orientated with one of the faces above, the average reaction rate inside the particle follows by integration using the Lambert–Beer law:

$$\frac{1}{d_p}\int_0^{d_p} r_j\,dx = k_j C_{sites} C_A^n (I''_s)^m \left\{\frac{1-\exp(-mb_{cat}d_p)}{mb_{cat}d_p}\right\} \quad (6)$$

where d_p is the catalyst particle size (m), T_p is the transparency of a single catalyst particle, and $b_{cat} = b(1-\varepsilon_p)$ is the extinction coefficient of the porous catalyst material (m^{-1}).

The transparency of a single catalyst particle, T_p, assuming the orientation described above, is given by

$$T_p = 1 - \exp(-mb_{cat}d_p) \quad (7)$$

From $m = 1$, $b_{cat} = 2.06 \times 10^6\ m^{-1}$, and $d_p = 3 \times 10^{-6}$ m, it follows that $T_p = 0.1$.

Due to the absorption of the UV light by the catalyst particles, the light flux will decrease down in the TIR. The light intensity in the reactor (I''_s), i.e. the light flux at the surface of the catalyst particle, is a function of the position of the catalyst particle in the reactor vessel and was obtained from the particle transparency by assuming the catalyst particles to be homogeneously distributed in the liquid and assuming a cylindrical reactor vessel geometry for simplicity:

$$\begin{aligned}\frac{I''_s(z)}{I''_0} &= \exp\left\{-\frac{N_p A_p (1-T_p)}{(1/4)\pi d_r^2}\left(\frac{h_L - z}{h_L}\right)\right\} \\ &= \exp\left\{-\frac{\left(((w_{cat}h_L(1/4)\pi d_r^2)/d_p^3\rho_{cat})\right)(d_p^2)(1-T_p)}{(1/4)\pi d_r^2}\left(\frac{h_L - z}{h_L}\right)\right\} \\ &= \exp\left\{-\frac{w_{cat}(1-T_p)(h_L - z)}{d_p\rho_{cat}}\right\}\end{aligned} \quad (8)$$

where z is the height from the bottom of the vessel (m), I''_0 is the irradiance at the liquid surface (Einst m^{-2} s^{-1}), N_p is the total number of catalyst particles in the vessel, A_p is the cross-sectional area of a catalyst particle, d_r is the diameter of the reaction vessel (m), w_{cat} is the catalyst concentration in the liquid (kg m^{-3}), ρ_{cat} is the catalyst particle density (kg m^{-3}) and h_L is the liquid height (m).

The relationship between the light intensity at the surface of the catalyst, $I''_s(z)$, and the irradiance at the liquid surface (top), I''_0 is given in Fig. 5 for various positions (height) in the TIR. A set of linear relations between I''_0 and $I''_s(z)$ is found. The transparency of the slurry is obtained from Eq. (8), using a catalyst concentration in the liquid of 1 g L^{-1} (or 1 kg m^{-3}), and a catalyst particle density of 1920 kg m^{-3}. The inset in Fig. 5 shows the decay in light intensity within the reaction medium in the TIR determined by Eq. (8). The light intensity I''_s drops down to half of its maximum at a penetration depth in the reaction medium of only 0.005 m. At the bottom of the reactor (0.054 m), the light reaching the catalyst surface is practically zero. This implies that effectively only the catalyst particles in the top of the vessel contribute to the conversion of the reactant! This is translating in the rapidly decreasing slope in the relation between I''_0 and $I''_s(z)$ at increasing liquid depth. Although the diameter of the lamp (d_{lamp} = 2.6 cm) is narrower than the reactor diameter ($d_{reactor}$ = 4.8 cm) it is for the modeling of the top-illuminated reactor for simplicity assumed that the average light intensity profile is determined by Eq. (8). In order to maintain the same amount of light shining into the reactor, the light intensity at the liquid surface in the modeling is multiplied by a factor $(d_{lamp}/d_{reactor})^2$.

The average reaction rate, expressed in $mol_A\ m_{cat}^{-3}\ s^{-1}$, follows from solving the integral in which $I''_s(z)$ in Eq. (6) is expressed using Eq. (8) and taking the average value in the reactor:

$$\frac{1}{h_L}\int_0^{h_L}\left(\frac{1}{d_p}\int_0^{d_p} r_j\,dx\right)dz = k_j C_{sites} C_A^n \left[\frac{(I''_0)^m}{mb_{cat}d_p}(1-\exp(-mb_{cat}d_p))\right] \left[\frac{d_p\rho_{cat}}{w_{cat}(1-T_p)h_L}\left\{1-\exp\left(-\frac{w_{cat}(1-T_p)h_L}{d_p\rho_{cat}}\right)\right\}\right] \quad (9)$$

3.3. IMMR

The incident photon flux emitted from the side light emitting fiber in perpendicular direction is radiated to the walls, assuming that the absorbance of light by the liquid and the gas in the channels is negligible. For calculation of the light distribution along the wall it is necessary to know the position of the fibers in the channels. At the top of the monolith most light-emitting fibers are

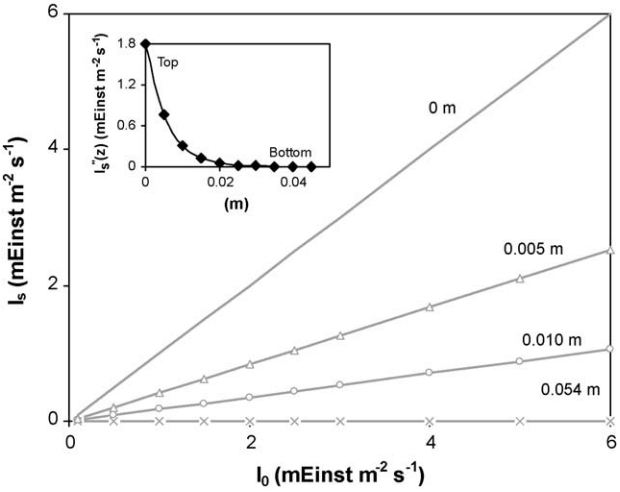

Fig. 5. Light intensity that reaches the catalyst surface (I_s) for both reactors for a given light intensity entering the reactor (I_0); for the TIR this dependency is different for a certain distance from the light source. The inset shows the light intensity decay in the TIR through the reaction mixture when I_0 is 1.8×10^{-3} Einst m^{-2} s^{-1}.

typically positioned in the corners of the monolith channels due to their stiffness. A closer look at the monolith, however, revealed that deeper in the channels most fibers are not located in the corners but at other positions nearby the wall. Since the precise position of the fibers does not have a tremendous influence on the light distribution over the perimeter of the channels provided that they are not fixed in the corners (in that case half of the light will be lost since there is no exchange of liquid in the small volume between the fiber and the wall), a rather simple geometry is assumed with the fibers touching the middle of the channel wall, as depicted in Fig. 6.

For simplicity, the fiber is considered as a small light source, assuming to have a very small radius, r_p. Since it can be assumed that the light intensity is equal in all directions, the light intensity at any position at the wall amounts to:

$$I_s'' = \frac{I_0'' r_f}{r_p} \times \frac{r_p \sin(\alpha_i)}{L_i} = I_0'' \frac{r_f \sin(\alpha_i)}{L_i} \tag{10}$$

where r_f is the fiber radius (m), r_p is the radius of (imaginary) light source in which the light emission is assumed to be concentrated (m), α_i is the angle of incident of the light onto the surface at section i (rad), and L_i is the distance between the light point source and section i of the wall surface (m).

The eccentric position of the fiber causes an unequal distribution of the light flux over the channel perimeter. In order to take that aspect into account without incorporating too much complexity, the wall perimeter is divided into segments, as depicted in Fig. 6. For each entire segment the distance from the light source and the angle of incident is set equal to the value in the middle of the segment. For segment 4 this is illustrated by the bold dashed line. For this segment, L_i and α_i follow from

$$L_i = \sqrt{\left(\frac{d_{ch}}{2} - \frac{d_f}{2}\right)^2 + \left(\frac{d_{ch}}{2}\right)^2} \text{ and } \tan(\alpha_i) = \frac{(1/2)d_{ch}}{(1/4)d_{ch}} = 2 \tag{11}$$

where d_{ch} is the channel width, and d_f is the fiber diameter ($=2 \times d_f$). A second fiber in the same channel is assumed to be located in the middle of the opposite wall. The local light intensity at all segments is then obtained by the sum of the light flux from both fibers. The procedure in which average values are used for the whole segment causes a slight deviation from the overall light flux balance. In order to achieve that the total amount of light emitted from the fibers is reached by the surface all around the channel a correction factor, c_f, is used:

$$I_0'' 2\pi r_f = 2 c_f I_0'' r_f \sum_{i=1}^{8} \left(w_i \frac{\sin \alpha_i}{L_i} \right) \tag{12}$$

where w_i is the width of wall segment i. The factor 2 in this equation accounts for the fact that the same 8 segments also occur on the top half of the channel. For the division in segments described above, a fiber diameter of 0.45 mm and an internal channel width of 0.43 mm, the value of c_f amounts to 1.12865.

The local light flux at the catalyst external surface thus becomes:

$$I_s'' = c_f I_0'' \frac{r_f \sin(\alpha_i)}{L_i} \tag{13}$$

From the surface of the catalyst to some depth (x) in a perpendicular direction the intensity will decrease according to:

$$I_x'' = I_s'' \exp\left(\frac{-b_{cat} x}{\sin(\alpha_i)} \right) \tag{14}$$

where I_x'' is the incident light flux at a depth x (Einst m^{-2} s^{-1}), x is the depth in the catalyst layer (distance to the external surface) (m) and b_{cat} is the extinction coefficient of the light in the (porous) catalyst layer (m^{-1}).

The equation for the reaction rate and the dependency on the light flux is given by Eq. (5). This expression is also valid in the IMMR. Since the penetration depth of the light into the catalyst layer is only about 2 μm the local reaction rate is given by Eq. (5). Since k_j, C_{sites}, C_A, and n and are constant over the depth into the catalyst layer, the average activity of the catalytic layer follows from the following integral over the depth of the layer:

$$\frac{1}{d_{cat}} \int_0^{d_{cat}} r_j \, dx = \frac{k_j C_{sites} C_A^n}{d_{cat} m b_{cat}} (I_s'')^m \left(1 - e^{((-m b_{cat} d_{cat})/\sin \alpha_i)} \right) \tag{15}$$

If there is more than one light fiber in the channel, the local light intensity will be the sum of that from all (k) fibers, resulting in

$$\frac{1}{d_{cat}} \int_0^{d_{cat}} r_j \, dx = \frac{k_j C_{sites} C_A^n}{d_{cat} m b_{cat}} \sum_k (I_{s,k}'')^m (1 - e^{((-m b_{cat} d_{cat})/\sin \alpha_{i,k})}) \tag{16}$$

Implementing Eq. (13) yields:

$$\frac{1}{d_{cat}} \int_0^{d_{cat}} r_j \, dx = \frac{k_j C_{sites} C_A^n}{d_{cat}} \frac{(c_f r_f I_0'')^m}{m b_{cat}} \sum_k \left\{ \left(\frac{\sin(\alpha_{i,k})}{L_{i,k}} \right)^m \left(1 - e^{((-m b_{cat} d_{cat})/\sin \alpha_{i,k})} \right) \right\} \tag{17}$$

This yields for the reaction rate, expressed in mol m_{cat}^{-3} s^{-1} :

$$\frac{1}{4 d_{ch} d_{cat}} \times \left\{ \int_0^{d_{cat}} r_j \, dx \right\} = k_j C_{sites} C_A^n \frac{(c_f r_f I_0'')^m}{4 m b_{cat} d_{ch} d_{cat}} \sum_{i=1}^{8} 2 w_i \sum_k \left\{ \left(\frac{\sin(\alpha_{i,k})}{L_{i,k}} \right)^m (1 - e^{((-m b_{cat} d_{cat})/\sin \alpha_{i,k})}) \right\} \tag{18}$$

The factor 2 in Eq. (18) accounts for the other half of the wall around (the eight sections account only for half of the wall around).

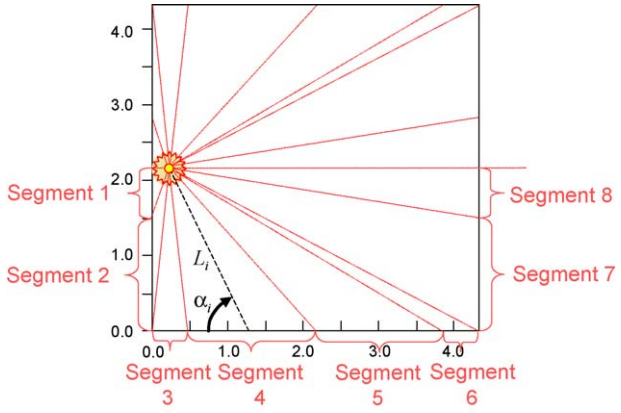

Fig. 6. Light directions considered in a monolith channel illuminated by one fiber. The figure also shows the division of the perimeter of the channel in segments used in the simulation. Segments 1 and 8 are set equal to 0.15w, segments 2 and 7 to 0.35w, segments 3 and 6 to the fiber diameter, and segments 4 and 5 to 0.5w minus the fiber diameter (with w = channel width).

4. Discussion

The value of k_j, Eq. (5), was estimated from the experimental results shown in Fig. 1b and the value found was 0.42 (Einst m^{-2} s^{-1})$^{-1}$ m^3 mol_A mol_{sites}^{-1} s^{-1} for $m = 1$. The catalyst used in both reactors for the experimental work was the same, so k_j will have the same value in both reactors, for a given m.

Table 1
Comparison of the two photoreactors in terms of photon flow (F_p), area from where the light enters the reactor (A), photon flux (I_0''), distance from light to catalyst surface, in the TIR is considered the distance between the top and bottom and the IIMR the channel diameter (h) and reactor length (L) for $m = 1$.

	F_p (Einst s^{-1})	A (m^2)	I_0'' (einstein m^{-2} s^{-1})	h (m)	L (m)	dn/dt (mol s^{-1})	ξ
IIMR	1.5×10^{-6}	3.00×10^{-2}	4.7×10^{-5}	4×10^{-3}	2.5×10^{-1}	1.7×10^{-8}	0.01
TIR	9.8×10^{-7}	5.40×10^{-4}	1.8×10^{-3}	5.5×10^{-2}	5.5×10^{-2}	1.2×10^{-8}	0.01

The photocatalytic reaction rate varies as a function of photon flux with an exponential factor m than can have values ranging from 0 to 1 [17]. The optimum light utilization corresponds to the domain where $m = 1$, where the photons used by the catalyst are limiting. The reaction rate is then fully proportional to the light intensity. Fig. 4 shows that the experiments were done in this domain. Since all the light emitted is absorbed by the catalyst on which the reaction can take place without diffusion limitation, the photonic efficiency follows directly from a very simple equation, see Eq. (19), independent of the reactor system:

$$\xi = \frac{k_j C_{sites} C_A^n}{b_{cat}} = 0.01 \tag{19}$$

Using the same value of k_j determined with the experimental data in the TIR, the results obtained previously in our laboratory [6] on the IIMR were simulated with the model developed. In Fig. 2b it is demonstrated that the simulated initial reaction rate is in accordance with the experimental values. The strong deactivation, evident from the deviation of linearity, was expected due to the strong product adsorption in the 80 μm catalytic layer [6].

When comparing both reactors, it is important to evaluate the way that the light is quantified. Table 1 summarizes the experimental conditions. The photon flow, F_p, which is proportional to the power emitted by the lamps, is approximately the same for both reactors. Since the area through which the light is dissipated in the reactor is much higher for the IIMR as compared to the TIR, the local light flux at the catalyst surface (I_s'', equaling I_0'' for the IIMR and the liquid surface of the TIR) is much lower in the IIMR. Still, because of the assumption that all photons will be absorbed, and taking into account that I_0'' values are in the regime where $m = 1$ for both reactors, the photonic efficiency is theoretically, and within the error of the measurement, the same.

Although in the presented data the reactors show the same performance, the conclusion should not be drawn that the reactors are as attractive. When higher light intensities are applied, m will be quite different in both reactors and the IMMR is superior because of the relatively low local light intensity. Moreover, the strong intensity profile in the TIR is very unfavourable: where the intensity is highest, m is lowest; more than half of the catalyst and reactor volume is not being used for the reaction. Thus, there is an advantage of an even light distribution, and as a result of this, a more efficient use of the light in the IIMR compared to the design where the photocatalyst is dispersed in the reaction medium (TIR). The optimal design corresponds to the IIMR where a layer of photocatalyst particles (with 5 μm thickness) is facing the light.

Finally, it is noted that the presence of bubbles in the IIMR will cause light refraction by the liquid (reactant) and reflection by the gas–liquid interface, probably causing a less equal distribution of the light over the channel perimeter. Since the reactor is operated in the film flow regime, the internal walls are likely to be covered with a liquid film. The liquid flows along the walls and the air in the center of the channel. The effect of this light refraction and reflection will be small if the reaction rate is approximately proportional to the light intensity, and it will be negligible if the rate is exactly proportional to the light intensity, i.e. $m = 1$.

Further research is currently in progress to investigate the dependency of the reaction rate with the light intensity and to obtain more detailed experimental results in the IIMR to demonstrate the advantages of that reactor system. The dependency of the factor m with light intensity needs to be further clarified for the both studied systems.

5. Conclusions

The experimental work in the TIR has resulted in a series of useful data on the catalytic selective oxidation of cyclohexane to cyclohexanone and cyclohexanol. The results were modelled successfully and the light-dependent reaction rate coefficient was estimated. Additionally a model was developed for simulation of the IIMR and the results were also modelled successfully.

The illuminated geometric surface in the IIMR is two orders of magnitude higher than in the TIR. So, for the same power (photon flow) entering each reactor the local light fluxes are much lower in the IIMR and, as a consequence, the IIMR operates at higher rates, because of a higher value of m, than the TIR for the same power delivered to both systems.

Moreover, the diameter of the catalyst layer in the IMMR is that low that the light intensity profile is much more favourable than that of the TIR, for which most of the reaction medium slurry is essentially dark. Together with the common advantages of immobilized systems, e.g. no catalyst separation difficulties, the IIMR design revealed to be superior compared to the TIR in terms of light usage by the catalyst.

References

[1] M.F.J. Dijkstra, H. Buwalda, A.W.F. de Jong, A. Michorius, J.G.M. Winkelman, A.A.C.M. Beenackers, Chem. Eng. Sci. 56 (2001) 547.
[2] H. de Lasa, M. Serrano, M. Salaices, Photocatalytic Reaction Engineering, Springer, New York, 2005.
[3] M. Schiavello, Heterogeneous Photocatalysis, Wiley, Chichester, 1997.
[4] H.F. Lin, K.T. Valsaraj, J. Appl. Electrochem. 35 (2005) 699.
[5] M.T. Kreutzer, F. Kapteijn, J.A. Moulijn, J.J. Heiszwolf, Chem. Eng. Sci. 60 (2005) 5895.
[6] P. Du, J.T. Cameiro, J.A. Moulijn, G. Mul, Appl. Catal. A 334 (2008) 119.
[7] C.B. Almquist, P. Biswas, Appl. Catal. A 214 (2001) 259.
[8] P. Boarini, V. Carassiti, A. Maldotti, R. Amadelli, Langmuir 14 (1998) 2080.
[9] C. Giannotti, S. Legreneur, O. Watts, Tetrahedron Lett. 24 (1983) 5071.
[10] J.M. Herrmann, W. Mu, P. Pichat, Stud. Surf. Sci. Catal. (1991) 405.
[11] G.X. Lu, H.X. Gao, J.H. Suo, S.B. Li, Chem. Commun. (1994) 2423.
[12] W. Mu, J.M. Herrmann, P. Pichat, Catal. Lett 3 (1989) 73.
[13] P. Du, J.A. Moulijn, G. Mul, J. Catal. 238 (2006) 342.
[14] T.A. Nijhuis, A.E.W. Beers, T. Vergunst, I. Hoek, F. Kapteijn, J.A. Moulijn, Catal. Rev. Sci. Eng. 43 (2001) 354.
[15] J.T. Carneiro, C.C. Yang, J.A. Moma, J.A. Moulijn, G. Mul, Catal. Lett. 129 (2009) 12.
[16] B. Mahltig, H. Bottcher, K. Rauch, U. Dieckmann, R. Nitsche, T. Fritz, Thin Solid Films 485 (2005) 108.
[17] J.M. Herrmann, Catal. Today 53 (1999) 115.
[18] J.E. Kroeze, T.J. Savenije, J.M. Warman, J. Am. Chem. Soc. 126 (2004) 7608.
[19] T.J. Savenije, M.P. de Haas, J.M. Warman, Int. J. Res. Phys. Chem. Chem. Phys. 212 (1999) 201.
[20] A.R. Almeida, J.A. Moulijn, G. Mul, J. Phys. Chem. C 112 (2008) 1552.